Experimental review of unpolarised nucleon structure functions

Vladimir Chekelian (Shekelyan)[a]

[a]Max-Planck-Institut für Physik (Werner-Heisenberg-Institut)
Föhringer Ring 6, 80805 München, Germany
E-mail: shekeln@mppmu.mpg.de

Recent results are reviewed on unpolarised structure functions from fixed target experiments at JLAB, NuTeV and from the HERA ep collider experiments H1 and ZEUS.

1. Introduction

The study of the structure of hadrons has been a powerful means for establishing and testing of the theory of strong interactions and for the determination of the partonic content of the nucleon. In 1969 the SLAC-MIT collaboration [1] observed the scaling behaviour [2] of the proton structure function in deep inelastic electron-proton scattering (DIS). This observation established the quark-parton model (QPM) as a valid framework for the interpretation of DIS data and that different partonic processes can be expressed in terms of universal parton densities. The smallness of $R = \sigma_L/\sigma_T$, the ratio of the cross sections from longitudinally and transversally polarised virtual photon scattering measured in DIS [3], provided the first evidence of the spin-1/2 nature of the partons. In 1974 in μN interactions [4] and in subsequent neutrino and muon-nucleon scattering experiments, the observation of scaling violation and the identification of partons as quarks and gluons has confirmed the field theory of quarks and gluons and their strong interactions, Quantum Chromodynamics (QCD).

The structure functions in QCD are defined as a convolution of the universal parton momentum distributions inside the proton and coefficient functions, which contain information about the exchanged boson-parton interaction. At sufficiently large four-momentum transfer squared, Q^2, when the strong coupling α_s is small, a perturbative technique is applicable for QCD calculations of the coefficient and splitting functions. The latter represent the probability of a parton to emit another parton. Expressions for structure functions are determined by convolution integrals of appropriate sums over the densities of quarks of different flavours and gluons, which predict a logarithmic Q^2 dependence (evolution) of the structure functions. The perturbative QCD (pQCD) calculations are well established within the DGLAP [5] formalism to next-to-leading (NLO) order in the strong coupling and have recently been extended to next-to-next-to-leading (NNLO) order [6].

In 2004 D. Gross, D. Politzer and F. Wilczek have been awarded the Nobel Prize for the discovery of asymptotic freedom. F. Wilczek in his brief commentary [7] on the QCD foundational papers wrote that the "most dramatic" experimental consequence "regarding the pointwise evolution of structure functions", namely "that the proton viewed at ever higher resolution would appear more and more as field energy (soft glue), was only clearly verified at HERA twenty years later". Indeed, the first measurements by the HERA electron proton collider experiments H1 and ZEUS in 1992 [8,9] revealed a steep rise of the proton structure function towards small x, the fraction of proton momentum carried by the parton. The present state of the art of these measurements [10–14] is shown in Figure 1 as a function of x at $Q^2 = 15$ GeV^2 (left figure) and as a function of Q^2 at different x values (right figure).

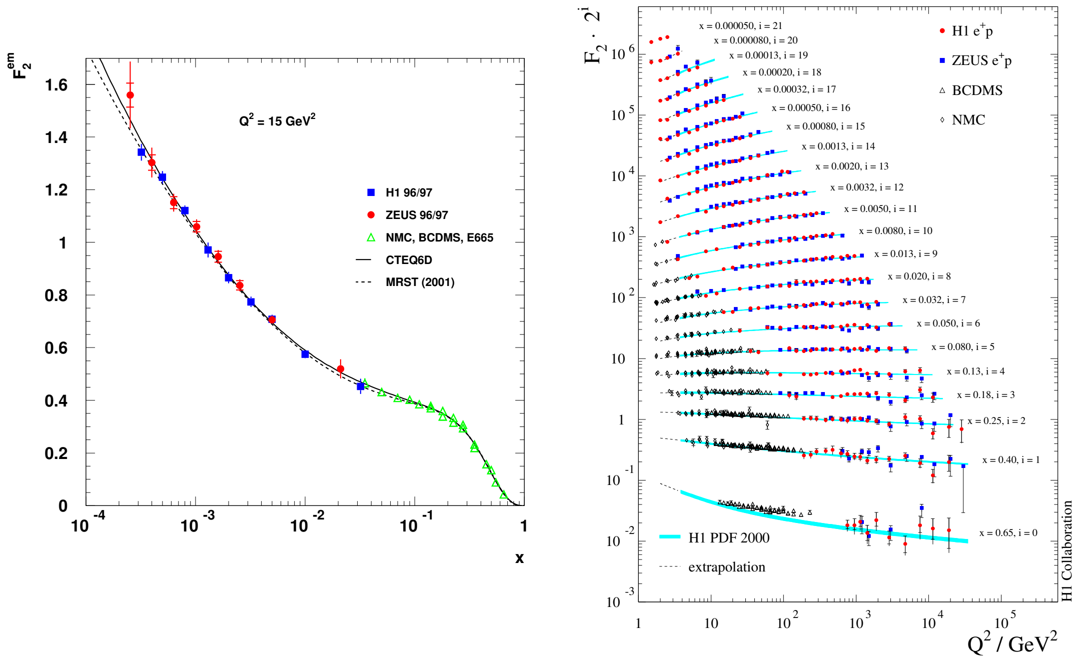

Figure 1. Proton structure function $F_2(x, Q^2)$ measured at HERA and in fixed target experiments as a function of x at $Q^2 = 15$ GeV^2 (left) and as a function of Q^2 for different x values (right). Curves represent different NLO QCD fits.

Partons, i.e. quarks and gluons, enter differently into different structure functions. In deep inelastic scattering the cross section of the neutral or charged current (NC or CC) process can be expressed in terms of three structure functions. For example for neutral current process mediated by γ or Z^o-boson exchange, the expression is

$$\frac{d^2\sigma^{e^\pm p \to e^\pm X}}{dx dQ^2} = \frac{2\pi\alpha^2}{Q^4 x}\left[Y_+ F_2(x, Q^2) - y^2 F_L(x, Q^2) \mp Y_- x F_3(x, Q^2)\right], \tag{1}$$

where $y = Q^2/xs$ is the inelasticity, s is the center of mass energy squared, α is the fine structure constant and $Y_\pm = 1 \pm (1-y)^2$. The dominant contribution to the cross section is due to the proton structure function F_2, which, in the framework of QPM, is related to the sum of the proton momentum fractions carried by the quarks and antiquarks in the proton weighted by the quark charges squared. The longitudinal structure function F_L, vanishing in QPM, is directly sensitive to the gluon momentum distribution in the proton. The structure function xF_3 depends on the valence quarks and is sizable only at large Q^2, when Q^2 is comparable with the Z^o-boson mass squared.

In this paper the recent JLab results on the transverse and longitudinal structure functions in the nucleon resonance region, the NuTeV measurements of the isoscalar structure functions $F_2(x, Q^2)$ and $xF_3(x, Q^2)$ in νFe interactions and the HERA results on structure functions are reviewed as presented at the BARYONS 2004 conference. The HERA results include analyses of the inclusive NC and CC $e^{\pm}p$ cross section measurements in the framework of perturbative NLO QCD, determination of the quark and gluon distributions inside the proton, results on the strong coupling obtained from inclusive and jet data and also measurements of the charm and beauty contributions to F_2.

2. Recent results from fixed target experiments

The Jefferson Lab experiment E94-110 measured inclusive scattering of unpolarised electrons off a hydrogen target in the nucleon resonance region, in the range $0.2 < Q^2 < 5.5$ GeV^2 [15]. The longitudinal-transverse separation allowed the proton structure functions $F_2 = (2xF_1 + F_L)/(1 + 4M^2x^2/Q^2)$, F_1 (purely transverse) and F_L (purely longitudinal) to be extracted independently. Here, M is the proton mass. The measurements of $2xF_1$ and F_L are shown in Figure 2 as a function of x for different Q^2 values. The longitudinal component is found to be significant, both structure functions show resonant mass structures which oscillate around the lines corresponding to QCD fits. At $Q^2 \geq 1.5$ GeV^2 the average x dependence of the resonance region is well described. The observed scaling relationship between resonance electroproduction and deep inelastic scattering, termed quark-hadron (Bloom-Gilman) duality [16], suggests a common origin for both kinematic regimes and brings additional information on the transition from soft to hard QCD. These data represent the first observation of duality in the separated transverse and longitudinal structure functions.

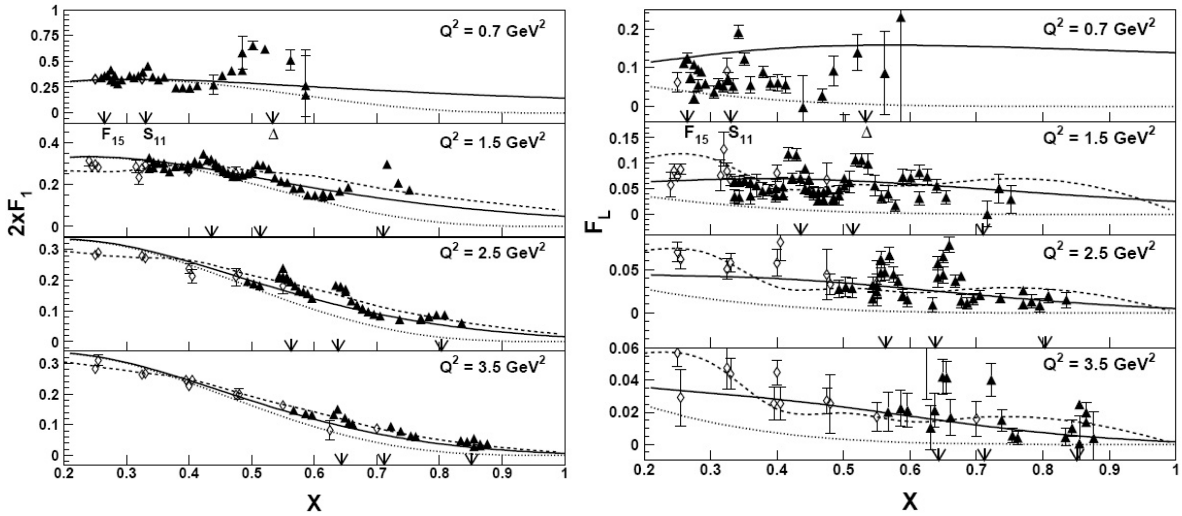

Figure 2. The transverse ($2xF_1$) and longitudinal (F_L) structure functions from the E94-110 experiment (triangles) compared with the SLAC measurements (diamonds) and the NNLO QCD fits from Alekhin [17] (dashed line) and MRST [18] (solid line) with, and MRST (dotted line) without target mass effects included. The prominent resonance mass regions are indicated by arrows.

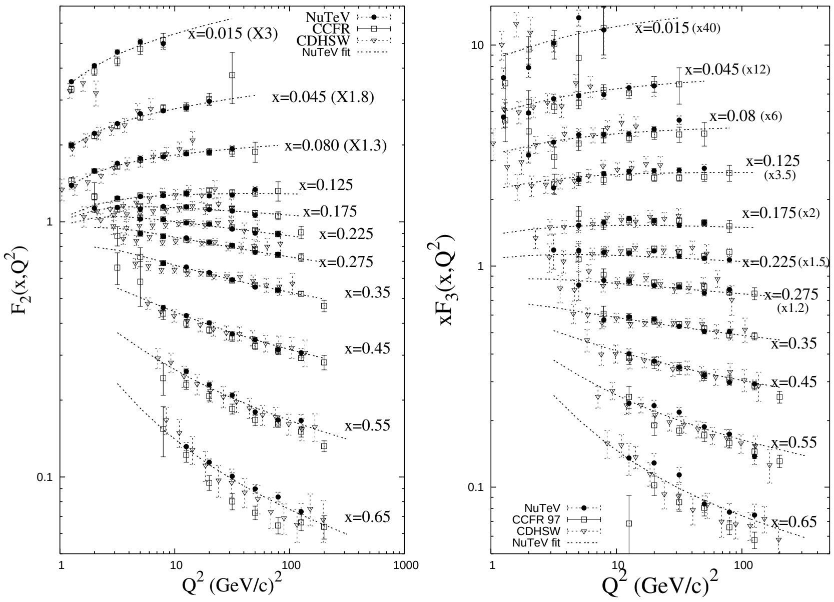

Figure 3. The NuTeV measurements of $F_2(x, Q^2)$ and $xF_3(x, Q^2)$ compared with the data from CCFR and CDHSW. The curve represents the fit to the NuTeV data.

The NuTeV experiment has obtained high statistics samples of neutrino and antineutrino CC interactions using the high energy sign-selected neutrino beam at Fermilab. Isoscalar neutrino-iron structure functions $F_2(x, Q^2)$ and $xF_3(x, Q^2)$ [19] determined by fitting the y dependence of the sum and the difference of ν and $\bar{\nu}$ cross sections are shown in Figure 3. The measurements benefit from the precise determination of muon and hadron energy scales (0.7% and 0.43%, respectively) obtained using continuous calibration beam running concurrently with the data taking. At intermediate x ($0.015 < x < 0.5$) both $F_2(x, Q^2)$ and $xF_3(x, Q^2)$ are in good agreement with the CCFR results which are also shown in Figure 3. At lowest x ($x = 0.015$) and in the high x region ($x > 0.5$) the NuTeV data are systematically above the CCFR results by ≈ 3 % and by up to ≈ 20 %, respectively. The new measurements have improved systematic precision, and they have expanded into the previously unaccessible kinematic range of high inelasticity y.

3. HERA results

The kinematic coverage of the HERA structure function measurements in the x-Q^2 plane is shown in Figure 4 (left). HERA extends the phase space of the previous fixed target measurements (also shown in the figure) by 2 orders of magnitude both in x and Q^2. The full HERA range in x is essential for predictions for the LHC collider.

At the HERA collider, the incident electron (or positron) energy is 27.6 GeV and the proton energy is 920 GeV (820 GeV till 1997), which correspond to a center of mass energy of 319 (301) GeV. In the first phase of data taking, HERA I, the H1 and ZEUS experiments each collected about 100 pb^{-1} of integrated luminosity in the e^+p mode and about 15 pb^{-1} in the e^-p mode. The H1 and ZEUS measurements of the single differential NC and CC $e^\pm p$ cross sections $d\sigma/dQ^2$ [13,14,20–22] are summarised in Figure 4 (right).

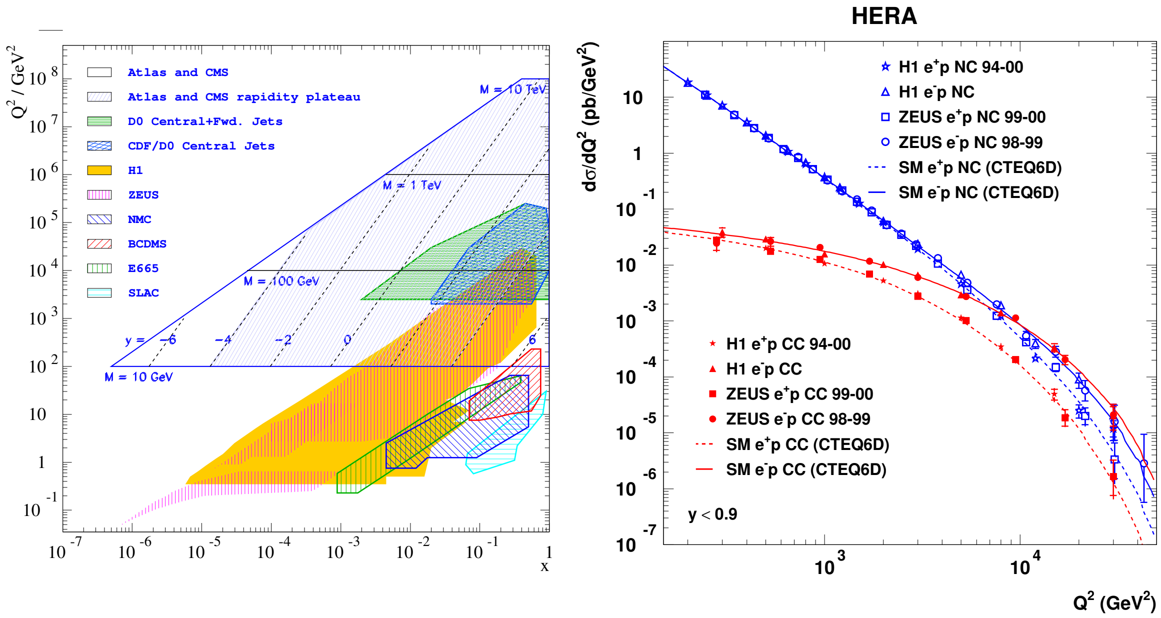

Figure 4. Kinematic reach at the HERA collider and in the fixed target experiments together with the regions of jet production in pp scattering (left). The H1 and ZEUS measurements of the NC and CC $e^{\pm}p$ cross sections as a function of Q^2 (right).

At low $Q^2 \approx$ 100 GeV^2 the cross section of the CC process mediated by the W boson, is smaller by 3 orders of magnitude than that of the NC process, due to the different propagator terms. At high $Q^2 \approx M_Z^2, M_W^2$ the cross section measurements are approaching each other demonstrating the unification of the weak and electromagnetic forces. From a comparison of the NC measurements at highest Q^2 with the Standard Model expectation, a limit on the quark radius of $\approx 10^{-18}$ m is obtained, proving a pointlike behaviour of quarks down to about 1/1000 of the proton radius.

3.1. Partonic structure of the proton

The measurements of the full set of NC and CC double differential $e^{\pm}p$ cross sections at HERA allow comprehensive QCD analyses to determine the quark and gluon distributions inside the proton and the strong coupling constant $\alpha_s(M_Z^2)$.

Double differential NC $e^{\pm}p$ cross section measurements at high x are shown in Figure 5 (left). At low Q^2 the cross sections of the e^+p and e^-p interactions are essentially indistinguishable. At high Q^2 they depart from each other due to the different sign of the xF_3 contribution to the cross section (see eq. 1). The HERA experiments determined the structure function xF_3 [13,22] by the difference of e^+p and e^-p cross sections. It is dominated by the $\gamma - Z$ interference term and depends on the valence quark density only. Double differential CC $e^{\pm}p$ cross sections are shown in Figure 5 (right) as a function of x for different Q^2. They are sensitive to individual flavours in the proton, the e^+p data to d and the e^-p data to u quarks. At high x, the contribution from the valence quarks dominates the cross section and allows a local extraction of u and d densities.

Using inclusive measurements of the NC and CC $e^{\pm}p$ cross sections, H1 and ZEUS performed NLO QCD fits [13,24], which lead to a quark flavour decomposition of parton densities. In the ZEUS fit their jet data are used as well. The quark and gluon distribu-

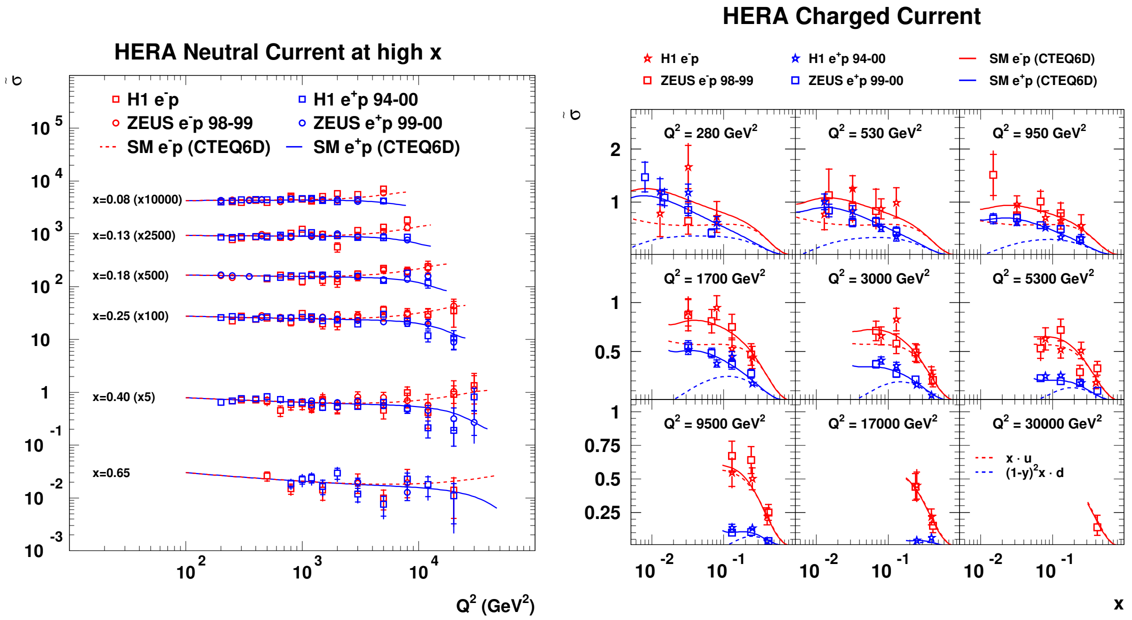

Figure 5. Double differential NC (left) and CC (right) $e^{\pm}p$ cross sections at HERA compared with the Standard Model predictions based on the CTEQ parton distributions [23]. For CC, the contributions from u and d quarks are also shown.

tions obtained in the H1 and ZEUS fits are shown in Figure 6 (left). The results agree within the quoted error bands. They agree also with the parton densities from global QCD fits [23,25] which include not only the HERA but also the fixed target DIS data as well as data from other processes sensitive to parton distributions, such as Drell-Yan, inclusive jet production and W-lepton asymmetry in $p\bar{p}$ collisions.

3.2. Low-x regime

The steep rise of the proton structure function at low x indicates a new partonic regime governed by a rising gluon density. This high parton density regime might reveal novel QCD effects, e.g. gluon-gluon recombination. The QCD analysis of inclusive measurements leads to a gluon distribution which rises towards small x at Q^2 above a few GeV^2, Figure 6 (right). At the lowest Q^2 the rise of F_2 persists, while the gluon density flattens out at $Q^2 \approx 2.5$ GeV^2 and even becomes dangerously close to zero at $Q^2 = 1$ GeV^2. This is not necessarily a problem in itself, since the gluon density from scaling violations is not an observable. A negative gluon density, however, would result in a distinct unphysical prediction for F_L. A closer look into the low x region is presented below in terms of derivatives of F_2 in $\ln x$ and $\ln Q^2$ and measurements of the longitudinal structure function F_L.

In the double asymptotic limit, the DGLAP evolution equation can be solved and F_2 is expected to rise approximately as a power of x towards low x. A power behaviour is also predicted in BFKL theory [26]. A damping of this rise would indicate the presence of novel QCD effects. A relevant observable for the investigation of the dynamics of this growth is the partial derivative of F_2 w.r.t. $\ln x$ at fixed Q^2, $\lambda = -(\partial \ln F_2(x,Q^2)/\partial \ln x)_{Q^2}$. The high precision of the present F_2 data allowed H1 to measure this observable locally [27]. The measurements are consistent with no dependence of λ on x for $x < 0.01$. Thus, the

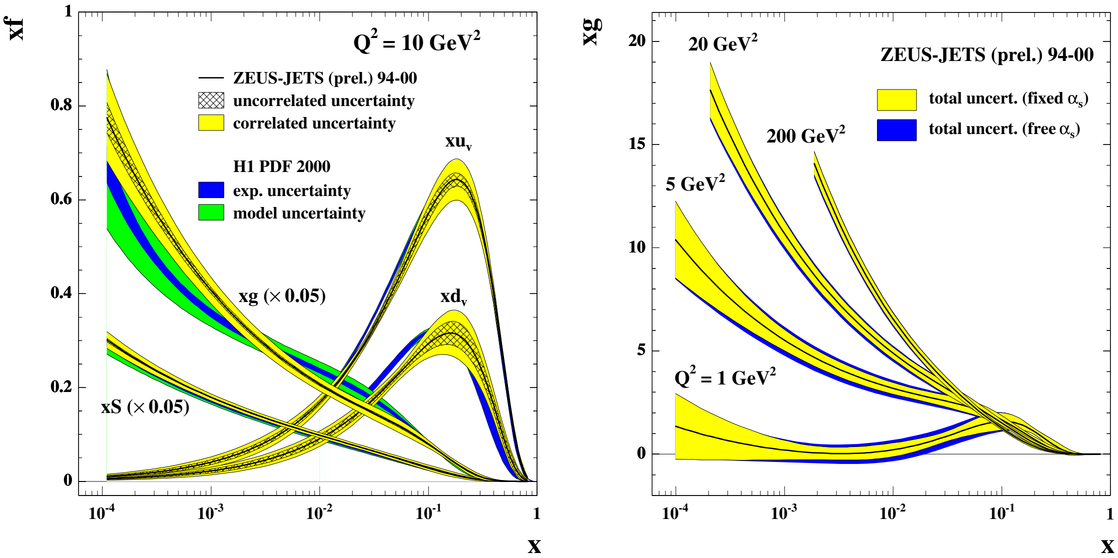

Figure 6. The valence, sea and gluon distributions as obtained from the H1 and ZEUS NLO QCD fits to NC, CC and jet data (latter in ZEUS fit only) at $Q^2 = 10$ GeV^2 as a function of x (left). The low x region is dominated by the gluon and sea quark distributions divided on the plot by a factor of 20. The gluon distribution from the ZEUS fit at Q^2 =1, 5, 20 and 200 GeV^2 (right).

monotonic rise of F_2 persists down to the lowest x measured at HERA, and no evidence for a change of this behaviour such as a damping of the growth is found. The observed independence of the local derivatives in $\ln x$ at fixed Q^2 suggests that F_2 can be parameterised in a very simple form $F_2 = c(Q^2)x^{-\lambda(Q^2)}$. The results for $\lambda(Q^2)$ obtained by H1 and ZEUS are shown in Figure 7 (left). The coefficient $c(Q^2) \approx 0.18$ and the parameterisation $\lambda(Q^2) = a{\cdot}\ln(Q^2/\Lambda^2)$ for $Q^2 \geq 2$ GeV^2 are consistent with pQCD analyses. At $Q^2 \leq 1$ GeV^2 the behaviour is changing, and, in the photoproduction limit ($Q^2 \approx 0$), λ is approaching 0.08, which is expected from the energy dependence of soft hadronic interactions $\sigma_{tot} \sim s^{\alpha_P(0)-1} \approx s^{0.08}$.

Another important quantity in view of possible non-linear gluon interaction effects is the derivative $(\partial F_2/\partial \ln Q^2)_x$ which is a direct measure of scaling violations. Its behaviour in x is a reflection of the gluon density dynamics in the associated kinematic range. The derivative measurements are shown in Figure 7 (right) as a function of x for different Q^2. They show a continuous growth towards low x without an indication of a change in the dynamics. The derivatives are well described by the pQCD calculations for $Q^2 \geq 3$ GeV^2.

Non-zero values of the structure function F_L appear in pQCD due to gluon radiation. Therefore, F_L is a most appropriate quantity to test QCD to NLO and especially to examine pathological effects related to a possibly negative gluon distribution. According to eq. 1, the F_L contribution to the inclusive cross section is significant only at high y. The conventional way to measure F_L is to explore the y dependence of the cross section at given x and Q^2 by changing the center of mass energy of the interaction. Such measurements are not yet performed at HERA. The H1 collaboration nevertheless could determine F_L from measurements at high y, i.e. small scattered electron energies down to 3 GeV. Various

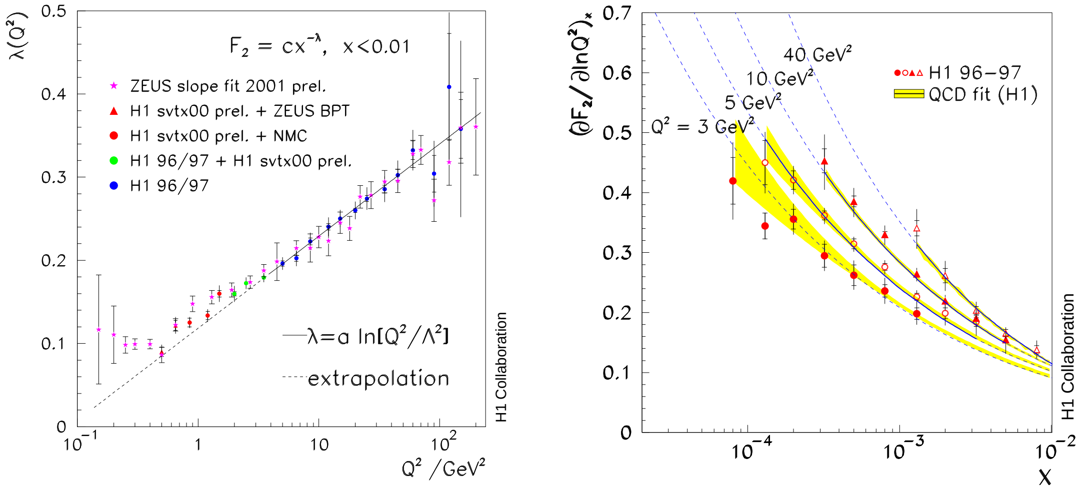

Figure 7. Fitted values of $\lambda(Q^2)$ (right). The derivative $(\partial F_2/\partial \ln Q^2)_x$ as a function of x for different Q^2 (right).

methods are used which attribute the observed decrease of the cross section at high y to F_L according to eq. 1. A summary of the F_L measurements by H1 [28] is shown in Figure 8 (left). The results are significantly above zero everywhere, including the lowest Q^2. They are compared with pQCD calculations and different phenomenological models showing that already at the present level of precision the measurements can discriminate between different predictions. Direct measurements of F_L at HERA can be performed only by reducing the beam energy and employing the highest y domain.

3.3. Strong coupling α_s

Further insight into the structure of the proton is obtained in semi-inclusive processes such as jet or heavy flavour production which are calculable in pQCD. The jet data have been included into the QCD analysis by ZEUS [24]. They help to reduce the uncertainty of the gluon distribution at medium x around 0.1. In this fit both, the gluon density shown in Figure 6 (right) and the fundamental coupling constant $\alpha_s(M_Z^2)$ were determined. The H1 collaboration has also performed a QCD fit [11] devoted especially to the determination of the gluon distribution and α_s. A novel flavour decomposition of F_2 used in this fit allows to reduce the number of parton distributions to just two combinations (apart from the gluon density): "valence-like" and "sea-like". The number of data sets can thus be reduced to a minimum, the H1 cross section data covering low x and the BCDMS μp data covering the region of large x. Without HERA data the gluon distribution from the fit to the BCDMS data becomes unrealistically flat at low x and drives $\alpha_s(M_Z^2)$ to about 0.110. The HERA data pin down the gluon density, and, as a result, $\alpha_s(M_Z^2)$ moves to 0.115 if both data sets are used.

The most precise HERA measurements of the strong coupling constant $\alpha_s(M_Z^2)$ in inclusive DIS are shown in Figure 8 (right) together with various $\alpha_s(M_Z^2)$ determinations from jet production at HERA [29]. The average $\alpha_s(M_Z^2)$ value in NLO from H1 and ZEUS is

$$\alpha_s(M_Z^2) = 0.1186 \pm 0.0011(exp) \pm 0.005(theory). \quad (2)$$

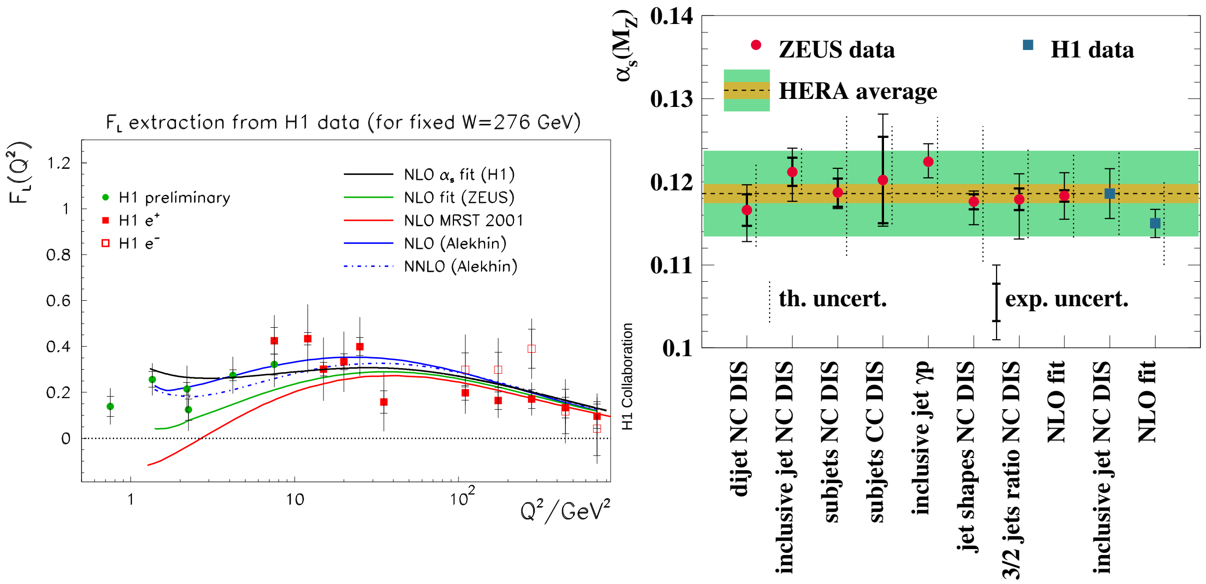

Figure 8. Summary of the F_L measurements by H1 at fixed photon-proton center of mass energy $W = 276$ GeV, $W \approx \sqrt{sy}$ (left). Measurements of the strong coupling constant $\alpha_s(M_Z^2)$ in inclusive DIS and jet production at HERA (right).

The experimental error is small, about 1%. A limitation of the precision of $\alpha_s(M_Z^2)$ arises from the associated theoretical error calculated using the *ad hoc* convention of varying the renormalisation and factorisation scales by a factor of 2. In forthcoming exact NNLO analyses the scale dependence will be considerably reduced. With theoretical and experimental progress in DIS, it is expected to pin down the least well-measured fundamental constant $\alpha_s(M_Z^2)$ to an accuracy of better than 0.001.

3.4. Heavy flavour production

The dominant heavy flavour production process at low x at HERA is photon-gluon fusion, in which a pair of charm or beauty quarks and antiquarks is produced. The mass of the heavy quark provides a hard scale and makes it possible to apply pQCD techniques for cross section calculations even in photoproduction ($Q^2 \approx 0$). The interplay between different hard scales, mass and p_t of the heavy quark and Q^2, is one of the questions which heavy flavour studies need to resolve.

Open charm production at HERA has mainly been studied by reconstructing D^* mesons which originate from the hadronisation of charm quarks and decay into $D^0\pi \to K\pi\pi$. The measured contribution of charm to the proton structure function [30,31] is shown in Figure 9 (left). The charm contribution is large and increases from $\approx 10\%$ at $Q^2 = 2$ GeV^2 to $\approx 30\%$ at $Q^2 = 500$ GeV^2. Silicon detectors surrounding the interaction region provide lifetime tagging for heavy flavour physics at HERA. Using this powerful tool the H1 collaboration determined the cross sections for charm and beauty production [32] shown in Figure 9 (right). The vertex tagged H1 charm data are consistent with the ZEUS D^* data and complement the data obtained at lower Q^2. The beauty contribution is about 1/10 of the charm contribution and amounts to about 2% of F_2. This is the first measurement of the beauty structure function $F_2^{b\bar{b}}$. The data are well described by pQCD

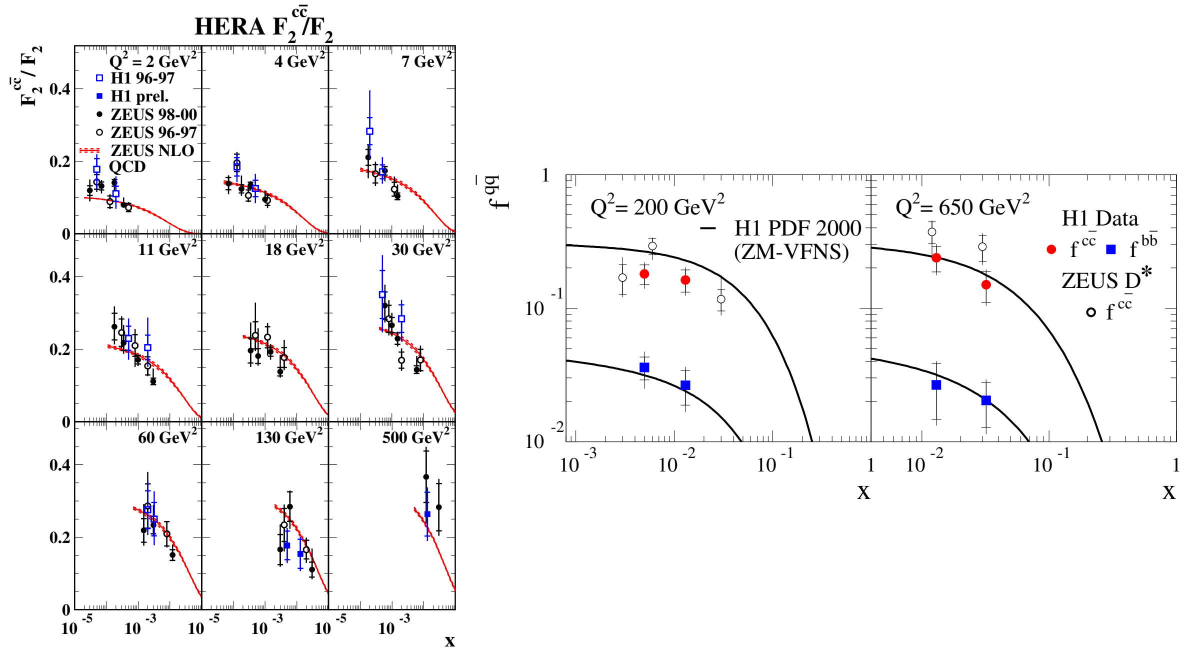

Figure 9. Fractional contributions of charm and beauty quarks to the proton structure function F_2. The curves correspond to predictions within the H1 and ZEUS QCD analyses.

calculations both for $F_2^{c\bar{c}}$ and $F_2^{b\bar{b}}$. The accurate measurement of these structure functions is important for the forthcoming LHC data, because their contribution is expected to be much increased for the scale relevant for the LHC.

3.5. First results from HERA II

Data taking of the second, high luminosity phase of the HERA program, HERA II, started in October 2003. After the upgrade of the collider the specific luminosity is increased by about a factor of 3. This was achieved by placing strong super-conducting focusing magnets inside the H1 and ZEUS detectors, close to the interaction point. In 2003-2004 HERA has delivered about 100 pb^{-1}. A major success at HERA II is the longitudinal polarisation of the positron beam (P), typically about 40%. This new feature was exploited by H1 and ZEUS to measure polarised NC and CC e^+p cross sections [33,34]. The measured total CC cross sections are shown in Figure 10 together with unpolarised HERA I data ($P = 0$). The measurements confirm the predicted linear dependence of the CC cross section on the longitudinal polarisation of the positron beam. The e^+p cross section is expected to vanish at $P = -1$ unless right handed weak currents exist. The result of the combined H1 and ZEUS cross section measurements, linearly extrapolated to $P = -1$, is $0.2 \pm 1.8(stat) \pm 1.6(syst)$ pb ($\chi^2/dof = 5.4/4$), which is consistent with absence of right handed weak currents.

4. Outlook

For more than three decades unpolarised structure function measurements in DIS are providing crucial experimental input to establish the quark parton model, to develop QCD and to determine universal parton distribution functions. The area is still very active and provides many results from fixed target experiments and, in the past decade,

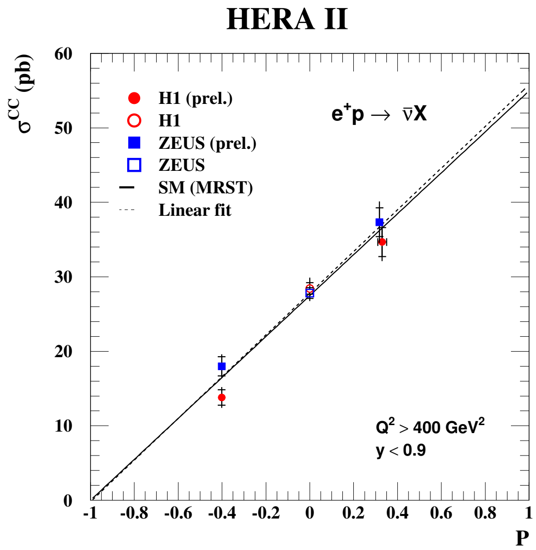

Figure 10. Measurements of the total CC e^+p cross section as a function of the positron beam polarisation P. The published HERA I results correspond to $P = 0$. The first preliminary HERA II measurements are made at $P = -0.40$ and $P = 0.33$. The lines indicate the Standard Model expectation and a linear fit to the data.

from the unique ep collider HERA. The second phase of the HERA program with increased luminosity and upgraded detectors just started. The rich physics program of HERA II has the goal to collect about 1 fb^{-1} of data, including a special run with lower proton beam energies for direct measurements of F_L at low x. The end of HERA, foreseen for mid 2007, will definitely not allow to complete the program and will enforce compromises on the physics outcome from HERA. The field has a large potential in a long term future. Extensions of the present HERA program to study neutron structure in ed collisions and for measurements at low x and Q^2 with improved precision have been proposed recently [35]. The HERA (or Fermilab) proton ring could serve for ep collisions with the future International Linear Collider at the new energy frontier [36]. Physics opportunities and the accelerator and detector options for a future Electron Ion Collider, EIC/eRHIC at BNL [37], are under discussion.

REFERENCES

1. E.D. Bloom et al., Phys. Rev. Lett. 23 (1969) 930;
   M. Breidenbach et al., Phys. Rev. Lett. 23 (1969) 935.
2. J.D. Bjorken, Phys. Rev. 179 (1969) 1547.
3. R.E. Taylor and F.J. Gilman, Proc. of the 4th Int. Symposium on Electron and Photon Interactions at High Energies, Liverpool 1969, ed. D.W. Braben, Daresbury (1970);
   W. Albrecht et al., DESY 69-46 (1969);
   A. Bodek et al., Phys. Rev. D 20 (1979) 1471.
4. D.J. Fox et al., Phys. Rev. Lett. 33 (1974) 1504.
5. Y. L. Dokshitzer, Sov. Phys. JETP 46 (1977) 641;
   V. N. Gribov and L. N. Lipatov, Sov. J. Nucl. Phys. 15 (1972) 438 and 675;

G. Altarelli and G. Parisi, Nucl. Phys. B 126 (1977) 298.
6. S. Moch, J. Vermaseren and A. Vogt, Nucl. Phys. 688 (2004) 101 and 691 (2004) 129.
7. http://web.mit.edu/physics/facultyandstaff/faculty_documents/wilczek_select_pubs.pdf
8. H1 Collab., I. Abt et al., Nucl. Phys. B 407 (1993) 515.
9. ZEUS Collab., M. Derrick et al., Phys. Lett., B 316 (1993) 412.
10. M. Klein, in proceedings of ICHEP'04, Beijing, 2004.
11. H1 Collab., C. Adloff et al., Eur. Phys. J. C 21 (2001) 33.
12. ZEUS Collab., S. Chekanov et al., Eur. Phys. J. C 21 (2001) 443.
13. H1 Collab., C. Adloff et al., Eur. Phys. J. C 30 (2003) 1.
14. ZEUS Collab., S. Chekanov et al., Phys. Rev. D 70 (2004) 052001.
15. Y. Liang et al., nucl-ex/0410027, submitted to Phys. Rev. Lett. (2004).
16. E.D. Bloom and F.J. Gilman, Phys. Rev. Lett. 25 (1970) 1140.
17. S. Alekhin, Phys. Rev. D 68 (2003) 0114002.
18. A.D. Martin, R.G. Roberts, W.J. Stirling, R.S. Thorne, Eur. Phys. J. C18 (2000) 117.
19. http://www-nutev.phyast.pitt.edu/results_2004/nutev_sf.html;
V.A. Radescu, hep-ex/0408006, in proceedings of DIS 2004, Strbske Pleso, Slovakia.
20. ZEUS Collab., S. Chekanov et al., Eur. Phys. J. C32 (2003) 1 and Phys. Lett. B 539 (2002), erratum in Phys. Lett. B 552 (2003) 308.
21. H1 Collab., C. Adloff et al., Eur. Phys. J. C 19 (2001) 269.
22. ZEUS Collab., S. Chekanov et al., Eur. Phys. J. C 28 (2003) 175.
23. J. Pumplin et al., JHEP 0207 (2002) 012.
24. ZEUS Collab., contributed paper to ICHEP'04, Beijing, 2004, abstract 5-0263.
25. A.D. Martin, R.G. Roberts, W.J. Stirling, R.S. Thorne, Eur. Phys. J. C 23 (2002) 73.
26. E.A. Kuraev, L.N. Lipatov and V.S. Fadin, Sov. Phys. JETP 44 (1976) 443;
E.A. Kuraev, L.N. Lipatov and V.S. Fadin, Sov. Phys. JETP 45 (1977) 199;
Y.Y. Balitsky and L.N. Lipatov, Sov. Journ. Nucl. Phys. 28 (1978) 822.
27. H1 Collab., C. Adloff et al., Phys. Lett. B 520 (2001) 183;
H1 Collab., contributed paper to EPS03, Aachen, 2003, abstract 082.
28. H1 Collab., contributed paper to ICHEP'04, Beijing, 2004, abstract 5-0161.
29. C. Glasman, Proc. of New Trends in HERA Physics 2003, eds. G. Grindhammer et al., World Scientific, Singapore (2004), p. 126, hep-ex/0312011;
A. Everett, in proceedings of ICHEP'04, Beijing, 2004.
30. H1 Collab., C. Adloff et al., Phys. Lett. B 528 (2002) 199.
31. ZEUS Collab., S. Chekanov et al., Phys. Rev. D 69 (2004) 0120004.
32. H1 Collab., A. Aktas et al., hep-ex/0411046, submitted to Eur. Phys. J. C.
33. H1 Collab., contributed paper to ICHEP'04, Beijing, 2004, abstract 4-0756.
34. ZEUS Collab., contributed paper to ICHEP'04, Beijing, 2004, abstract 5-0257.
35. T. Alexopoulos et al., eD scattering with H1, a Letter of Intent, DESY 03-194;
H. Abramowicz et al., A new experiment for HERA, MPP-2003-62.
36. The THERA book, eds. U. Katz, A. Levy, M. Klein and S. Schlenstedt, DESY-01-123-F vol. 4, LC-REV-2001-062 (2001).
37. http://www.phenix.bnl.gov/WWW/publish/abhay/Home_of_EIC/